Quantum Chemical and Statistical Rate Study of the Reaction of O(3 P) with Allene: O-Addition and H-Abstraction Channels

ARTICLE *in* THE JOURNAL OF PHYSICAL CHEMISTRY A · DECEMBER 2006

Impact Factor: 2.69 · DOI: 10.1021/jp0639905 · Source: PubMed

3 AUTHORS, INCLUDING:

Thanh Lam Nguyen
University of Texas at Austin
72 PUBLICATIONS **1,377** CITATIONS

SEE PROFILE

Jozef Peeters
University of Leuven
205 PUBLICATIONS **4,431** CITATIONS

SEE PROFILE

Quantum Chemical and Statistical Rate Study of the Reaction of O(^{3}P) with Allene: O-Addition and H-Abstraction Channels

Thanh Lam Nguyen, Jozef Peeters, and Luc Vereecken*

Department of Chemistry, University of Leuven, Celestijnenlaan 200F, B-3001, Leuven, Belgium

Received: June 26, 2006; In Final Form: September 1, 2006

The lowest-lying triplet and singlet potential energy surfaces for the O(^{3}P) + CH_2=C=CH_2 reaction were theoretically characterized using the complete basis set model chemistry, CBS-QB3. The primary product distributions for the multistate multiwell reactions on the individual surfaces were then determined by RRKM statistical rate theory and weak-collision master equation analysis using the exact stochastic simulation method. The results predict that the electrophilic O-addition pathways on the central and terminal carbon atom are dominant up to combustion temperatures. Major predicted end-products for the addition routes include CO + C_2H_4, $^3CH_2$ + H_2CCO, and CH_2=C$^\bullet$−CHO + H$^\bullet$, in agreement with experimental evidence. CO + C_2H_4 are mainly generated from the lowest-lying singlet surface after an intersystem crossing process from the initial triplet surface. Efficient H-abstraction pathways are newly identified and occur on two different electronic state surfaces, ^{3}A″ and ^{3}A′, resulting in OH + propargyl radicals; they are predicted to play an important role at higher temperatures in hydrocarbon combustion chemistry and flames, with estimated contributions of ca. 35% at 2000 K. The overall thermal rate coefficient k(O + C_3H_4) at 200−1000 K was computed using multistate transition state theory: $k(T) = 1.60 \times 10^{-17} \times T^{2.05} \times \exp(-90\ \mathrm{K}/T)$ cm^3 molecule^{-1} s^{-1}, in good agreement with experimental data available for the 300−600 K range.

I. Introduction

Chemical processes occurring in combustion and flames go through complex reaction networks normally consisting of several hundreds and even thousands of coupled elementary reactions. Characterizing the dominant elementary reactions is very important to understand the overall reaction mechanisms, with the ultimate goal of optimizing the combustion process. It is well-known that small unsaturated hydrocarbons such as C_2H_2, C_2H_4, C_3H_4, and C_3H_6 are crucial intermediates in hydrocarbon-fueled flames.[1,2] Major, if not dominant, consumption pathways of these small unsaturated hydrocarbons are their reactions with triplet ground-state oxygen atoms. These reactions also play an important role in the generation of polycyclic aromatic hydrocarbons (PAH) and soot precursors. In previous papers, the reactions of C_2H_2,[3] C_2H_4,[4] and C_2F_4[5] with O(^{3}P) were theoretically characterized using high-level state-of-the-art calculations. Our predicted reaction mechanisms, product distributions, and thermal rate coefficients are in good agreement with the available experimental data. In this paper, we address the reaction of allene with triplet oxygen atom.

The O(^{3}P) + allene reaction was extensively studied experimentally.[6−15] Various reaction channels leading to different primary products were observed and are summarized below; where possible, the experimental reaction enthalpies[16] at 0 K are indicated, with computed values at the CBS-QB3 level given in parentheses for the purpose of comparison (kcal/mol).

O(^{3}P) + CH_2=C=CH_2

→ CO + $^1C_2H_4$	−119.6	(−119.6)	(1)
→ $^3CH_2$ + H_2CCO	−24.4	(−23.6)	(2)
→ H$^\bullet$ + CH_2=C$^\bullet$−CHO		(−14.0)	(3)
→ cyclopropanone		(−99.9)	(4)
→ allene oxide		(−90.0)	(5)
→ acrolein		(−120.4)	(6)
→ $^\bullet C_2H_3$ + HC$^\bullet$O	−24.0	(−24.9)	(7)
→ C_2H_2 + H_2CO	−77.6	(−77.5)	(8)
→ $H_2C^\bullet$−C≡CH + $^\bullet$OH	−12.9	(−12.8)	(9)

To our knowledge, the H-abstraction channel (9) has not been considered before; our predictions (see below) suggest it plays an important role in high-temperature conditions. Even though reaction channel (1) is a spin-forbidden process, all earlier experiments[7−12] showed CO plus singlet ethene to be the most important products for the title reaction. This channel was believed[7−12] to occur via an addition mechanism of triplet oxygen on the central carbon in allene and to go through vibrationally hot, long-lived, singlet cyclopropanone formed after intersystem crossing (ISC) from the starting triplet to the lowest-lying singlet surfaces. Primary ketene formation (channel 2) was detected in matrix studies of the reaction between allene and triplet oxygen atoms produced in the photolysis of ozone.[9] The products H$^\bullet$ + allenyloxy radical from channel (3) and

* Corresponding author fax: int-32-16-327992; e-mail: Luc.Vereecken@chem.kuleuven.be.

10.1021/jp0639905 CCC: $33.50
Published on Web 10/18/2006

•C_2H_3 + HC•O from channel (7) are thought to arise from the O-atom addition step on the terminal carbon.[10] Furthermore, in experimental matrix studies[9] cyclopropanone, allene oxide, and acrolein were stabilized and observed as final products. However, only a small amount of acrolein was detected in xenon matrices, in good agreement with an earlier study in the gas phase.[7] Finally, trace amounts of formaldehyde, likely arising from channel (8), were observed.[9]

Thermal rate coefficients for the O(^{3}P) + allene → products were measured at low and moderate temperatures (T < 900 K).[13−15] From these data, the experimental Arrhenius activation energy was derived to be about 1.85 ± 0.2 kcal/mol;[6] at room temperature, a rate of ca. 1.3×10^{-12} cm^3 molecule^{-1} s^{-1} was recommended.[6]

There are two published theoretical studies of the O(^{3}P) + allene reaction. Chiu and Abidi[17] explained the spin-forbidden reaction channel (1) using self-consistent theory, while Lester and co-workers[18] investigated the O-atom attack on the central and terminal carbon atoms in allene using the CASSCF(6,6)/DZP level of theory. The latter authors computed the barrier heights for these two steps to be 15 and 17 kcal/mol, respectively. These values overestimate the experimental data by ∼14 kcal/mol, primarily because the CASSCF method does not include dynamic electron correlations.

From the above we see that the mechanism of the O(^{3}P) + allene reaction appears to be very complicated, consisting of parallel and coupled reaction channels as well as ISC processes. In this context, high-level quantum chemical calculations in combination with accurate statistical kinetic analysis are necessary in order to better understand the reaction mechanisms as well as the formation of the major products of the title reaction.

II. Methodology

II.1. Quantum Chemical Calculations. Geometries of stationary points on the triplet and singlet surfaces were optimized at the hybrid density functional B3LYP/6-311G(d,p) level of theory,[19,20] followed by analytical frequency calculations at the same level to verify the stationary points located (one imaginary frequency for a transition structure and all positive frequencies for a minimum). Intrinsic reaction coordinate (IRC)[21,22] calculations were also performed at this level to establish the correct connections between the reaction intermediates, in some cases enhanced by G2M single-point calculations on the B3LYP geometries to refine the potential energy curves; all IRC calculations are shown in Figures S19−S41 in the Supporting Information. To obtain more accurate relative energies for the relevant intermediates, TS and products, the complete basis-set model chemistry CBS-QB3[23] was used. Table 1 shows that the CBS-QB3 results are in good agreement with the available experimental data; the discrepancy compared to experiment is about 1−2 kcal/mol. CBS-QB3 works fairly well for equilibrium structures where wave functions commonly have single-reference character. For transition structures, where the breaking of old bonds and the formation of new bonds occur simultaneously, the wave functions are more likely to have multireference character or suffer from near degeneracy effects; i.e., the nondynamic electronic correlations become important; this is often indicated by a high-spin contamination. In this work, we used the CASSCF[24,25] method to analyze the wave functions for kinetically important minima and transition states showing a high-spin contamination in the single-reference treatment. The configuration interaction (CI) vectors from these computations are presented in Table S4 (see the Supporting Information) and show that the highest CI coefficients, i.e., the contributions of the most important configuration, are >0.9 for all species considered, indicating that the HF-configuration is dominant and hence that the single-reference method CBS-QB3 is expected to yield reasonable results.

To investigate the proximity or possible crossing of the triplet and singlet potential energy curves as a function of the OCC angle in •OCH_2•CCH_2 species, or the CCC angle in •CH_2C-(=O)CH_2• species, we used the CASSCF(8,8)/cc-pVDZ level of theory to optimize geometries at each fixed OCC (or CCC) angle, while other coordinates in •OCH_2•CCH_2 (or •CH_2C(=O)-CH_2•) species were allowed to relax freely. Energies were subsequently refined employing the CASPT2(8,8)/cc-pVDZ level[26] based on the CASSCF reference wave function, thereby taking dynamic electron correlations into account.

The DFT-B3LYP and CBS-QB3 calculations were performed using the Gaussian 03 package,[27] while the CASSCF and CASPT2 calculations used the Dalton[28] and Molpro[29] packages; all optimized geometries, harmonic vibration frequencies, rotational constants, and energies are given in the Supporting Information.

II.2. RRKM/Master Equation Calculations. Product distributions as a function of temperature and pressure (P = 1 atm, T = 300−2000 K) for the O(^{3}P) + allene reaction proceeding on the triplet and singlet surfaces—considered as being adiabatic—were separately obtained by solution of the weak-collision master equation using Gillespie's exact stochastic simulation method,[30−32] explained in detail in our earlier paper[33] and discussed briefly here. In the energy-grained master equation, the ceiling energy considered was 200 kcal/mol above the initial adduct (e.g. triplet biradical **Int1a**), and a small energy band size of 0.03 kcal/mol (10 cm^{-1}) was chosen to ensure that the density of states does not change significantly within the band. To obtain the product distribution with high statistical precision, a large number of stochastic trials of ∼10^7 was used. In this application, the Mersenne Twister (MT19937)[34] random number generator was used.

The Lennard-Jones collision parameters for bath gas He are σ = 2.55 Å and ϵ/k_B = 10 K.[35] Since no collision parameters for [C_3H_4O] are available in the literature, the values σ = 4.08 Å and ϵ/k_B = 421 K are estimated based on those of ethylene oxide C_2H_4O.[35] Thus, the collision frequency Z_{LJ} [M] was estimated at ≈1.1×10^{10} s^{-1} at 1 atm and room temperature. The probability density function for collisional energy transfer was computed using the biexponential model of Troe.[36] An average energy transferred per collision $\langle \Delta E \rangle_{all}$ of −130 cm^{-1} was adopted. The initial energy distribution of formation of the triplet •CH_2C(=O)C•H_2 adduct **Int1a** from O(^{3}P) + allene via **TS1a** was derived from detailed balance considerations.[37]

The statistical RRKM theory[37−42] of unimolecular reaction rates is used to compute the energy−specific rate constants $k(E)$ for a reactant with an internal energy E

$$k(E) = \frac{\alpha}{h} \times \frac{G^{\ddagger}(E - E^{\ddagger})}{\rho(E)} \qquad (10)$$

where α is the reaction pathway degeneracy, h is Planck's constant, $E^{\ddagger}$ is the barrier height for the reaction, $G^{\ddagger}(E-E^{\ddagger})$ is the sum of vibrational states of the transition state (TS) for energies from 0 up to $E-E^{\ddagger}$, and $\rho(E)$ is the density of states for a reactant molecule with internal energy E. The Beyer−Swinehart−Stein−Rabinovitch algorithm[43,44] was used to calculate the sum and density of states in eq 10 employing a grain size of 0.003 kcal/mol (1 cm^{-1}).

TABLE 1: Total Energy (Hartrees) Including ZPE Corrections Calculated at the CBS-QB3 Level of Theory and Corresponding Relative Energy (kcal/mol) for Various Species in the $O(^3P) + CH_2{=}C{=}CH_2$ Reaction[e]

species	total energy	relative energy	exptl[d]
$O(^3P) + CH_2{=}C{=}CH_2$	−191.407952	0.0	0.0
$HCO + C_2H_3$	−191.447709	−24.9	−24.0 ± 1.6
$C_2H_2 + H_2CO$	−191.531528	−77.5	−77.6 ± 0.5
$CO + {}^1C_2H_4$	−191.598601	−119.6	−119.6 ± 0.4
$^3CH_2 + H_2CCO$	−191.445622	−23.6	−24.4 ± 1.0
$HCCO(X^2A'') + CH_3$	−191.453521	−28.6	−29.2 ± 1.4
$OH + H_2CCCH(C_{2v},{}^2B_1)$	−191.428384	−12.8	−12.9 ± 1.5
$H + CO + C_2H_3$	−191.424757	−10.5	−9.0 ± 1.1
$^1H_2CC + H_2CO$	−191.462174	−34.0	
$^3H_2CC + H_2CO$	−191.386907	13.2	
$CO + {}^3C_2H_4$	−191.492672	−53.2	
$CO + {}^3CH_3CH$	−191.483104	−47.2	
$CO + {}^1CH_3CH$	−191.479133	−44.7	
$H + H_2CCHCO$	−191.457397	−31.0	
$H + H_2CCCHO(C_s,{}^2A'')$	−191.430238	−14.0	
$H + H_2CCCHO(C_s,{}^2A')$	−191.423338	−9.7	
$H + CH_3CCO$	−191.441714	−21.2	
$H + HCCCH_2O$	−191.386875	13.2	
$H_2 + H_2CCCO$	−191.530180	−76.7	
$Int1a(C_{2v},{}^3B_2)$	−191.517546	−68.8	
$Int1b(C_{2v},{}^3B_1)$	−191.486270	−49.1	
$Int2a(C_s,{}^3A'')$: cis $^{\bullet}OCH_2{}^{\bullet}C{=}CH_2$	−191.446695	−24.3	
$Int2a(C_s,{}^3A'')$: trans $^{\bullet}OCH_2{}^{\bullet}C{=}CH_2$	−191.445006	−23.3	
$Int2b(C_s,{}^3A')$	−191.437097	−18.3	
Int3: $CH_3{-}C(=O){-}CH$	−191.496225	−55.4	
Int4	−191.483514	−47.4	
Int5: cyc-$CH_2OC^{\bullet}{-}{}^{\bullet}CH_2$	−191.451344	−27.2	
Int6: $^{\bullet}CH_2O^{\bullet}C{=}CH_2$	−191.447832	−25.0	
Int7: $^{\bullet}CH_2{}^{\bullet}CHCHO$	−191.502742	−59.5	
Int7: $^{\bullet}CH_2{}^{\bullet}CHCHO$	−191.489004	−50.9	
Int8: $^{\bullet}CH_2CH_2{}^{\bullet}C{=}O$	−191.506178	−61.6	
Int9: trans-$CH_3{}^{\bullet}CH{}^{\bullet}CO$	−191.522602	−71.9	
Int9: cis-$CH_3{}^{\bullet}CH{}^{\bullet}CO$	−191.522458	−71.9	
Int10: cis-CH_3CCHO	−191.497396	−56.1	
Int10: trans-CH_3CCHO	−191.494944	−54.6	
$Int11(C_{2v},{}^1A_1)$		−67.0[a]	
Int12: cyclopropanone	−191.567162	−99.9	
Int13: allene oxide	−191.551301	−90.0	
Int15: methyl ketene	−191.599289	−120.1	
Int16: trans-acrolein	−191.599743	−120.4	
Int16: cis-acrolein	−191.596458	−118.3	
$TS1a(C_s,{}^3A'')$	−191.406607	0.8; 0.9[c]	
$TS1b(C_s,{}^3A')$		3.5[c]	
$TS2a(C_s,{}^3A''$	−191.406043	1.2; 1.4[c]	
$TS2b(C_s,{}^3A')$		3.1[c]	
$TS3a(C_s,{}^3A'')$	−191.396312	7.3	
$TS3b(C_s,{}^3A')$	−191.392722	9.6	
TS4	−191.434020	−16.4	
TS5	−191.434847	−16.9	
TS6	−191.425495	−11.0	
TS7	−191.424484	−10.4	
TS8	−191.428845	−13.1	
TS9	−191.427161	−12.1	
TS10	−191.433200	−15.8	
TS13	−191.417779	−6.2	
TS14	−191.417175	−5.8	
TS15	−191.451302	−27.2	
TS16	−191.446861	−24.4	
TS17	−191.441421	−21.0	
TS18	−191.444961	−23.2	
TS20	−191.482837	−47.0	
TS22	−191.457033	−30.8	
TS23		−43.3[c]	
TS24	−191.455750	−30.0	
TS31		−65.5[b]	
TS32	−191.503085	−59.7	
TS33	−191.509124	−63.5	
TS34	−191.482013	−46.5	
TS35	−191.465968	−36.4	
TS37	−191.456414	−30.4	
TS38	−191.484775	−48.2	

[a] Derived from the relative energy of −68.8 kcal/mol for triplet oxyallyl and a triplet−singlet energy gap for oxyallyl of ca. 1.8 kcal/mol.[50] [b] Derived from a relative energy of −67.0 kcal/mol for singlet biradical oxyallyl and a barrier height of 1.5 kcal/mol computed at the UB3LYP/6-311G(d,p) level of theory. [c] Obtained from IRCMax(CBS-QB3:B3LYP) calculations. [d] Mainly taken from the Web page: http://srdata.nist.gov/cccbdb/. All values were obtained at 0 K: $\Delta H^0_f(O) = 58.98$ kcal/mol; $\Delta H^0_f(C_2H_2) = 54.48 \pm 0.2$ kcal/mol; $\Delta H^0_f(H) = 51.63$ kcal/mol; $\Delta H^0_f(CH_2{=}C{=}CH_2) = 47.4 \pm 0.3$ kcal/mol; $\Delta H^0_f(CH_2(X^3B_1)) = 93.2 \pm 0.5$ kcal/mol; $\Delta H^0_f(CO) = -27.2$ kcal/mol; $\Delta H^0_f(OH) = 8.84 \pm 0.1$ kcal/mol; $\Delta H^0_f(H_2CO) = -25.1 \pm 0.1$ kcal/mol; $\Delta H^0_f(C_2H_4) = 14.6 \pm 0.1$ kcal/mol; $\Delta H^0_f(CH_3) = 35.8 \pm 0.1$ kcal/mol; $\Delta H^0_f(C_2H_3) = 73.0 \pm 0.8$ kcal/mol; $\Delta H^0_f(HCO) = 9.95 \pm 0.1$ kcal/mol; $\Delta H^0_f(H_2CCCH) = 85.2 \pm 1$ kcal/mol;[47] $\Delta H^0_f(H_2CCO) = -10.66 \pm 0.3$ kcal/mol; $\Delta H^0_f(HCCO) = 42.0 \pm 1$ kcal/mol. [e] Where possible, data are also given derived from experiment-based 0 K enthalpies in the literature.

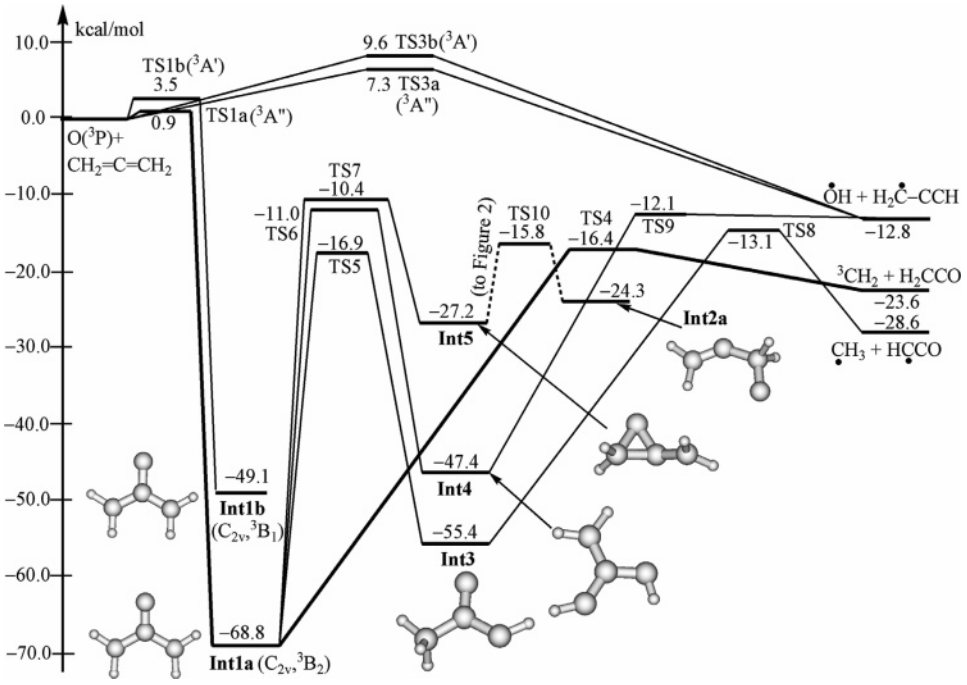

Figure 1. Section of the triplet potential energy surfaces starting from O-addition on the central carbon atom in CH_2═C═CH_2. Major pathway is indicated in bold. Two H-abstraction channels of the O + C_3H_4 reaction are also indicated. The dashed lines in the center connect to the PES section of Figure 2.

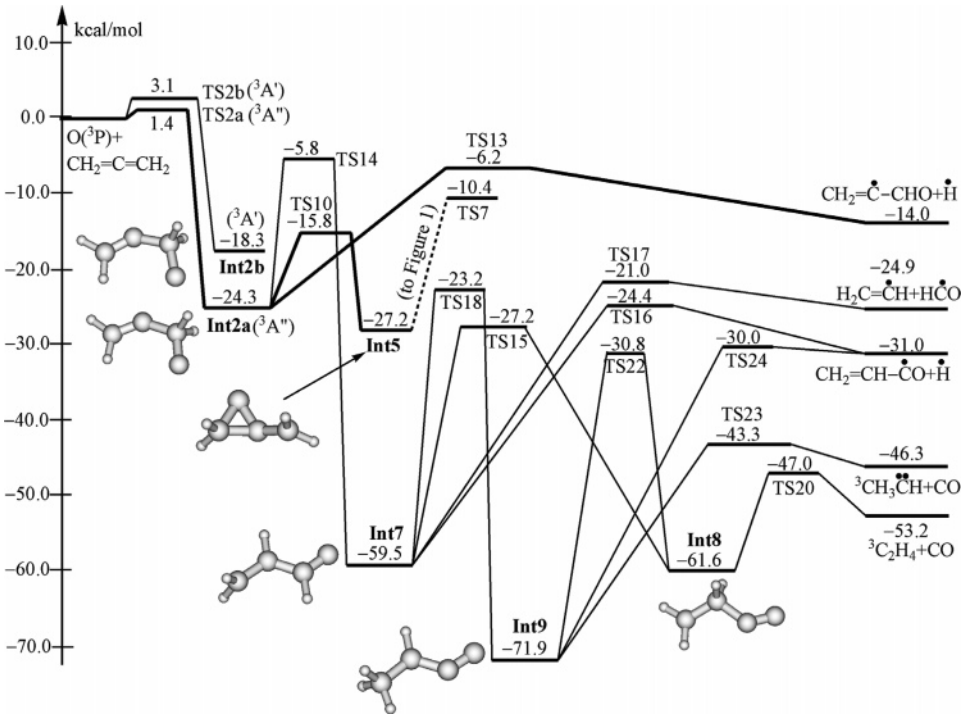

Figure 2. Section of the triplet potential energy surfaces starting at the O-addition on a terminal carbon atom in allene. Major pathways are indicated in bold. The dashed lines in the center connect to the PES section of Figure 1.

III. Results and Discussion

III.1. Potential Energy Surfaces. As first reaction step occurring on the triplet surface, the triplet O-atom can either attack on the central or the terminal carbon atom or abstract an H-atom from allene. We will discuss these three reaction pathways separately. Unless mentioned otherwise the relative energies obtained at the CBS-QB3 level of theory were used in the following discussion.

Figures 1 and 2 show part of the triplet potential energy surface for the reaction of triplet oxygen atom with allene, each starting from a different addition channel: O-attack on the central carbon (Figure 1) or O-addition on the terminal carbon (Figure 2). Transition states connecting these two regions of the PES are shown in both figures. The singlet PES is drawn in Figure 3. Some of the pathways we characterized are too high in energy to compete and are not shown in Figures 1−3; we refer to Figures S16−S18 in the Supporting Information for the complete surfaces. Ball-and-stick models of all minima and TS are depicted in Figures S8 and S9 in the Supporting Information. During the discussion we will indicate the dominant

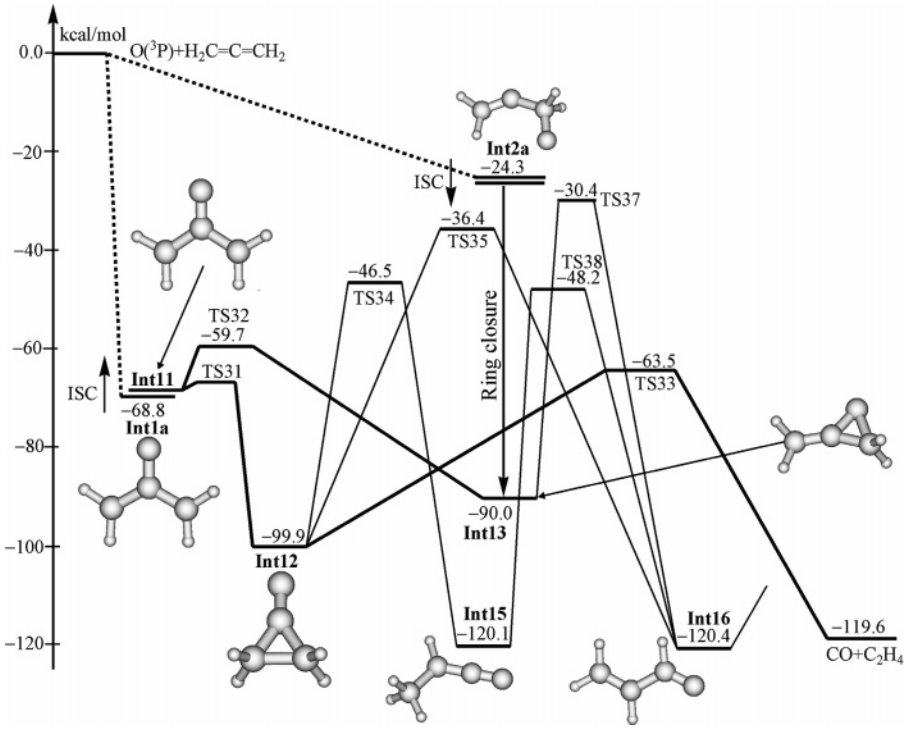

Figure 3. Singlet potential energy surfaces for the $O(^3P) + CH_2{=}C{=}CH_2$ reaction. Intersystem crossing from triplet to singlet surface (ISC) is indicated by arrows. The reaction channels on the triplet surface leading to the ISC starting intermediates are shown by dashed lines. Major pathways are indicated in bold.

pathways; the relative importance of a reaction channel is determined not only by the barrier height of the TS but also by the rigidity of the TS, i.e., its "looser" or "tighter" entropic characteristics, as well as by the available excess energy in chemically activated unimolecular reactions. Information on the relative rigidity of TS and on the effect of chemical activation was obtained in the master equation analyses discussed later and is used qualitatively in this section.

O-Atom Attack on the Central Carbon. Addition of the O-atom on the central carbon atom can occur on two different electronic-state surfaces, $^3A''$ and $^3A'$, via **TS1a**($^3A''$) and **TS1b**($^3A'$) leading to adducts **Int1a**($^3B_2$) and **Int1b**($^3B_1$), respectively (see Figure 1). These steps face barriers of 0.9 and 3.5 kcal/mol height, respectively. IRC calculations imposing a C_s symmetry indicate that **TS1a**($^3A''$) and **TS1b**($^3A'$) correlate to **Int1b**($^3B_1$) and **Int1a**($^3B_2$), respectively (see Figure S10), such that the two curves, $^3A''$ and $^3A'$, have to cross somewhere, around a C−O bond distance of 1.7 Å. In reality, the reaction proceeds on surfaces without symmetry constraints, and these two curves avoid crossing when relaxation of symmetry from C_s to C_1 is allowed (see Figure S11).

Triplet biradicals **Int1a**($^3B_2$) and the first electronically excited state **Int1b**($^3B_1$) lie 68.8 and 49.1 kcal/mol, respectively, below the initial reactants. The main differences between these two states is the location of the two unpaired electrons, so it is interesting to briefly discuss the shape of the two partly single occupied molecule orbitals (SOMO) in **Int1b**, especially as they change the geometry of **Int1b** compared to **Int1a**. One SOMO orbital of **Int1b**, formed by a combination of two P_x(C) orbitals located at two different carbon centers (see Figure S12), is perpendicular to the molecular plane of symmetry, such that the electron is delocalized along the CCC backbone. This results in the calculated C−C bond distance of 1.393 Å, i.e., closer to a double than a single C−C bond length. The second SOMO orbital lies in the molecular plane of symmetry and is located at the O-atom. So, the C−O bond distance elongates to 1.333 Å, ∼0.1 Å longer than a normal >C═O double bond. Attempts to locate TS from this electronically excited **Int1b** leading to (electronically excited) isomers or directly to products, including e.g. $CH_3 + HCCO(A^2A')$, were unsuccessful. By analogy with the **Int1a** reactions, the relevant barriers are expected to lie higher than the entrance TS, such that redissociation back to the initial reactants would be the dominant fate. Also, many of the isomerization pathways for **Int1b** would merge with the pathways of **Int1a** due to a lowering/changing of the symmetry around the TS, such that the kinetic behavior is essentially the same as if internal conversion (IC) to the lower electronic surface first took place. As a result, **Int1b** is modeled to undergo internal conversion to the lower electronic surface (**Int1a**) even at the highest temperatures, since the redissociation via **TS1b** back to the initial reactants at the average internal energy ($k(\langle E\rangle) \sim 10^{10}$ s^{-1} with $\langle E\rangle = 98$ kcal/mol at 2000 K, i.e., 49 kcal/mol above the initial reactants) is much slower than the IC, with the rate estimated at 10^{12} s^{-1}.[45,46]

Triplet biradical **Int1a** belongs to the C_{2v} point group. Its first SOMO orbital is similar to the first SOMO in **Int1b**, but the shapes of the second SOMO orbitals are completely different (see Figure S12). In **Int1a** it is formed by a linear combination of P_x(C), P_x(C), and P_x(O) orbitals located at three different atomic centers. As a consequence, both unpaired electrons in **Int1a** are delocalized over the molecule, and the C−O bond length, 1.266 Å, is closer to a double bond than in **Int1b,** while the C−C bond length, 1.466 Å, is closer to a single than a double C−C bond. Starting at **Int1a**, there are five different reaction pathways, namely the following: (i) CH_2-loss via **TS4** to yield triplet methylene plus ketene, needing to overcome a barrier of 52.4 kcal/mol height; (ii) a 1,3 H-shift via **TS5** to isomerize to **Int3**, facing a barrier of 51.9 kcal/mol; (iii) rearrangement to **Int4** via **TS6** with a barrier of 57.8 kcal/mol by a 1,3 H-shift from a carbon to the oxygen atom; (iv) ring-closure leading to **Int5** via **TS7**, over a barrier of 58.4 kcal/mol; (v) and finally, redissociation back to the initial reactants, which however cannot

compete with the former reactions because of its high barrier of 69.7 kcal/mol.

Int3, lying 55.4 kcal/mol below the initial reactants, either breaks the C−C bond to yield methyl plus ketenyl radicals via **TS8** or isomerizes back to **Int1a** via **TS5**. The barrier heights for the former and latter pathways are 42.3 and 38.5 kcal/mol, respectively. Although **TS8** lies 3.8 kcal/mol higher than **TS5**, the former is much looser, such that these two pathways should be competitive. **Int4**, 47.4 kcal/mol below the initial reactants, decomposes more easily to hydroxyl plus propargyl radical via the looser **TS9** than its rearrangement back to **Int1a** via the tighter **TS6**. The decomposition via **TS9** faces a barrier of 35.3 kcal/mol. **Int5** will undergo the ring-opening process via **TS10** with a small barrier of 11.4 kcal/mol, leading to **Int2a**. This intermediate is more closely related to addition reactions on the central carbon (see Figure 2), and its subsequent reactions are discussed in the next section.

In summary, the O-addition on the central carbon atom in allene results initially in the formation of both the triplet biradical adducts, **Int1a** and **Int1b**, of which the latter rapidly carries out an IC process to yield **Int1a**. When the spin is conserved throughout the reaction, decomposition of **Int1a** into triplet methylene plus ketene is expected to be dominant. Other decomposition channels could contribute but are expected to play a very minor role. It should be mentioned that the product ketene was experimentally observed earlier.[9] Reactions following an intersystem crossing to the singlet surface are discussed in a later subsection.

O-Atom Attack on a Terminal Carbon. IRC calculations show that the O-addition on the terminal carbon atom in allene proceeds through two different transition structures, **TS2a**(^{3}A″) and **TS2b**(^{3}A′), giving rise to triplet biradical adducts **Int2a**(^{3}A″) and **Int2b**(^{3}A′), respectively (see Figures S13 and 2). The barrier heights computed for these two steps are 1.4 and 3.1 kcal/mol.

Int2b(^{3}A′) has a relative energy of −18.3 kcal/mol with respect to the initial reactants and belongs to a C_s point group. Both SOMO orbitals carrying the two unpaired electrons in **Int2b** lie in the molecular plane of symmetry. One orbital is located on the O-atom, while the other is on the central carbon atom (see Figure S14). As for **Int1b**, the electronically excited **Int2b** can either undergo an internal conversion (IC) to the lower-lying electronic state (**Int2a**), redissociate to the original reactants, or undergo further unimolecular reactions (dissociation or isomerization). As seen for **Int2a**, the TS for these latter processes all break the symmetry, merging the A′ and A″ surfaces such that these reactions are similar to reactions after IC. While we cannot a priori quantify the rate of IC, it is expected to be dominant at low to moderate temperatures ($T \leq$ 1000 K), whereas redissociation is expected to become favorable only at very high temperatures ($T \geq$ 3000 K). The calculated energy-specific rate coefficient at the average energy for the redissociation step of **Int2b** sharply increases as a function of temperature, for example from 5.2×10^9 s^{-1} at $T = 1000$ K, passing through 3.3×10^{10} s^{-1} at $T = 1500$ K, and to 1.2×10^{11} s^{-1} at $T = 2000$ K. Therefore, the IC process should strongly compete with the redissociation, except at the highest temperatures.

Int2a, −24.3 kcal/mol relative to the initial reactants, possesses a ^{3}A″ symmetry in the C_s point group. In **Int2a**, one SOMO orbital lies in the molecular symmetry plane at the central carbon atom, while the other SOMO orbital is perpendicular to the molecular plane and located on the O-atom (see Figure S14), resulting in an additional stabilization of 6 kcal/mol for **Int2a** compared to **Int2b**. The chemically activated triplet adduct **Int2a** can eliminate an H-atom to give rise to allenyloxy radical + H products. This pathway goes through a loose transition structure **TS13** after clearing a barrier of 18.1 kcal/mol height. **Int2a** can either proceed through a ring-opening process leading to **Int5** via **TS10** or concertedly undergo a 1,2 H-migration and a ring-opening to **Int7** via **TS14**. The barrier heights are 8.5 and 18.5 kcal/mol, respectively. **Int5**, −27.2 kcal/mol relative to the initial reactants, will rearrange to **Int1a** via **TS7** by ring-opening. This pathway needs to overcome a barrier of 16.8 kcal/mol and leads to intermediates already discussed earlier (see Figure 1). Still, rearrangement of **Int5** back to **Int2a** via **TS10** is more favorable, in view of the lower barrier of 11.4 kcal/mol.

Int7, with relative energy 59.5 kcal/mol below the initial reactants, has four different accessible reaction pathways, namely the following: (i) H-elimination to yield H$^\bullet$ + CH$_2$═CH−$^\bullet$CO via **TS16**, needing to overcome a barrier of 35.1 kcal/mol; (ii) C−C bond rupture to produce $^\bullet$C$_2$H$_3$ + HC$^\bullet$O via **TS17** after clearing a barrier of 38.5 kcal/mol height; (iii) rearrangement by 1,2-H migration to **Int8** via **TS15** with a barrier of 32.3 kcal/mol; and finally, (iv) a 1,3 H-shift to give rise to **Int9** via **TS18**, the barrier height of which is 36.3 kcal/mol. Next, **Int9**, −71.9 kcal/mol compared to the initial reactants, can either decompose to triplet CH$_3$CH plus CO via **TS23** by C−C bond rupture or to H$^\bullet$ + CH$_2$═CH−$^\bullet$CO via **TS24** by H-loss. These pathways face barriers of 28.6 and 41.9 kcal/mol, respectively. **Int9** could undergo a 1,2 H-shift leading to **Int8** through **TS22** after clearing a high barrier of 41.1 kcal/mol. Because **TS23** is the lowest and loosest TS, the **Int9** → **TS23** → ^{3}CH$_3$CH + CO channel is expected to be the dominant decomposition channel of **Int9**. **Int8**, −61.6 kcal/mol relative to the initial reactants, will immediately break the single C−C bond via a very low-lying **TS20** to yield triplet ethylene plus CO. This step faces a low barrier of only 14.6 kcal/mol, indicating that rearrangement back to **Int7** or **Int9** is unlikely.

In summary, the O-addition on the terminal carbon atom in allene gives rise to the vibrationally excited, triplet biradical adducts **Int2a** and **Int2b**. Under conditions of low to moderate temperatures, **Int2b** will rapidly undergo an IC process to **Int2a**, whereas at higher temperatures **Int2b** redissociates back to the initial reactants in competition with the IC process. **Int2a**, in turn, will mostly decompose to allenyloxy plus hydrogen atom. The **Int2a** → **Int5** → **Int1a** → ^{3}CH$_2$ + ketene pathway is also expected to play an important role, indicating that the triplet surface for the O-attack on the terminal and central carbon atoms cannot be divided into independent site-specific regions. The products allenyloxy radical plus hydrogen atom were observed in molecular beam experiments by Lee and co-workers,[10] while ketene was detected in an experimental matrix study.[9] The **Int2a** → **TS14** → **Int7** step cannot compete with the two former channels; as a result, other products (including CO + ^{3}C$_2$H$_4$ and CO + ^{3}CH$_3$CH) produced from **Int7** on the triplet PES in Figure 2 can only be very minor. This result reconfirms the experimental studies,[7−11] which concluded that the product CO should be formed from a singlet intermediate after an ISC process from triplet to singlet surfaces.

The H-Abstraction. The O-atom can abstract an H-atom in allene yielding hydroxyl plus propargyl radical; the reaction has a calculated exothermicity of 12.8 kcal/mol, in excellent agreement with the experimental $\Delta_r H$(0 K) value of −12.9 kcal/mol.[16,45] This pathway can proceed via two transition structures of different electronic states, **TS3a**(^{3}A″) and **TS3b**(^{3}A′), correlating directly with the hydroxyl radical with a $^2\Pi$ symmetry (see Figure 1). The barrier heights for these channels are 7.3

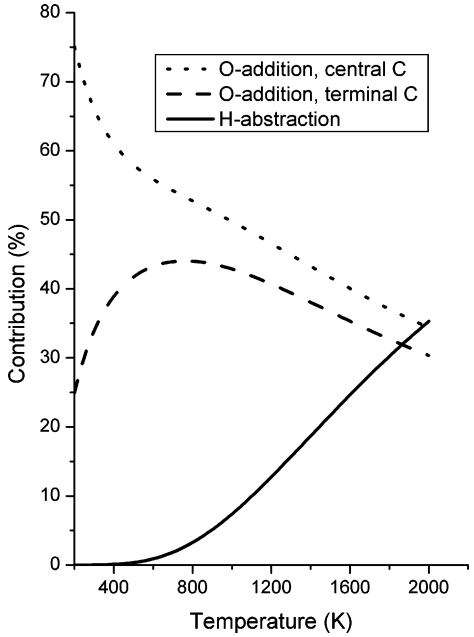

Figure 4. Calculated fractions of the H-abstraction and the site-specific O-addition reaction fluxes as a function of temperature (not corrected for redissociation).

and 9.6 kcal/mol, respectively, about 5−6 kcal/mol higher in energy than the O-addition transition structures. Consequently, the H-abstraction channel cannot compete with any of the O-addition channels at low to moderate temperatures but may play a role at combustion temperatures. To the best of our knowledge, all experimental studies for the title reaction were carried out at either low and moderate temperatures ($T <$ 900 K)[13−15] or at moderate collision energies in molecular beam experiments.[10] As a consequence, the products hydroxyl and propargyl radical were never observed. It is of interest to know how important the H-abstraction flux is compared to the total chemical reaction flux at higher temperatures. For this purpose, the fraction of H-abstraction flux as a function of temperature is computed using eq 11 based on TST considerations and plotted in Figure 4.

$$F_{\mathrm{H-abstraction}} = \frac{P_{\mathrm{H-abs}}}{P_{\mathrm{O-add-cen}} + P_{\mathrm{O-add-ter}} + P_{\mathrm{H-abs}}} \quad (11)$$

with

$$P_{\mathrm{H-abs}} = \kappa_{\mathrm{TS3a}} \times Q^{\ddagger}_{\mathrm{TS3a}} \times \exp(-E_{\mathrm{TS3a}}/RT) + \kappa_{\mathrm{TS3b}} \times Q^{\ddagger}_{\mathrm{TS3b}} \times \exp(-E_{\mathrm{TS3b}}/RT)$$

$$P_{\mathrm{O-add-cen}} = Q^{\ddagger}_{\mathrm{TS1a}} \times \exp(-E_{\mathrm{TS1a}}/RT) + Q^{\ddagger}_{\mathrm{TS1b}} \times \exp(-E_{\mathrm{TS1b}}/RT)$$

and

$$P_{\mathrm{O-add-ter}} = Q^{\ddagger}_{\mathrm{TS2a}} \times \exp(-E_{\mathrm{TS2a}}/RT) + Q^{\ddagger}_{\mathrm{TS2b}} \times \exp(-E_{\mathrm{TS2b}}/RT)$$

where Q_{TS} is the complete partition function of the given TS, R is the universal gas constant, E_{TS} is the energy of transition structure TS relative to the initial reactants, and κ_{TS3} is the one-dimensional tunneling correction for H-abstraction, which is computed by assuming an asymmetric Eckart potential.[48,49] It should be mentioned that the reaction pathway degeneracy derived from the symmetry numbers in the partition function for rotation is equal to 4 for each of the three reaction channels. This is obvious for the H-abstraction (4 equivalent hydrogens) and still easy to see for the addition to the terminal carbons (CH_2 groups): there are two of these carbons, and attack can come from two sides, exactly equivalent for each of the lobes of the π-bond. For the central C, there are 4 equivalent directions of attack, two for each of the two π-bonds it participates in.

As can be seen in Figure 4, the fraction of the H-abstraction flux depends strongly on temperature, i.e., ∼0% at 300 K, 4% at 900 K, and rising to ∼35% at 2000 K, indicating that the H-abstraction reaction channels can contribute significantly at combustion temperatures. In contrast, the fraction of O-addition on the central carbon atom steeply decreases with increasing temperatures, from 75% at 300 K to 35% at 2000 K. Nonetheless, it remains the most important reaction flux in much of the relevant temperature range. Temperature-dependence of the fraction of the O-addition on the terminal carbon is more complicated. First, it sharply rises with temperature and reaches a maximum of 45% around $T = 800$ K and then almost linearly decreases when temperature increases further. Still, throughout the 300−2000 K range, this channel contributes 30−45%. Note that taking into account the variational character of the low-barrier transition states for addition should even increase somewhat the calculated contribution of H-abstraction at high temperatures.

The Lowest-Lying Singlet Surface. The CBS-QB3 results for the triplet surface and statistical-kinetics predictions of the product distribution (see next sections) show that CO production from the triplet surfaces has a very small yield (<2%) under all relevant conditions. Yet, all experimental studies[7−12] find CO to be the most important product. Hence, the title reaction cannot take place only on the triplet surfaces but must also involve the (lowest-lying) singlet surface following an ISC process.

For the O-addition on the central carbon atom, a crossing region between triplet and singlet surfaces is expected in the vicinity of the equilibrium structure of triplet biradical adduct **Int1a,** because the triplet−singlet energy gap of oxyallyl is very small, 1−2 kcal/mol as already computed by Coolidge et al.[50] at the MRCI level of theory. To investigate the proximity of the triplet and singlet potential energy curves, we examine the energies of oxyallyl as a function of the CCC angle in the 90−140° range, i.e., the degree of freedom in which the triplet (**Int1a**) and singlet (**Int11**) oxyallyl species differ most and where facile cyclization to cyclopropanone might distort the PES most. We carried out geometry optimizations at several fixed CCC angles for a triplet wave function, while allowing the remaining 3N-7 internal coordinates in oxyallyl to relax freely; we then also used the same geometries to calculate the energies for a singlet wave function, allowing us to examine the energy difference for a vertical transition from triplet to singlet surface. The obtained results plotted in Figure 5 show that the triplet and singlet curves are close, within a few kcal/mol, for all CCC angles. Triplet oxyallyl is predicted to be the ground state, with a triplet−singlet energy splitting of only 1 kcal/mol, in good agreement with the reported MRCI result.[50] Therefore, in addition to reactions of triplet oxyallyl **Int1a** on the triplet surface, **Int1a** has a fair probability to undergo an intersystem crossing process to vibrationally excited singlet oxyallyl. Oxyallyl geometries reoptimized for singlet wave functions at fixed CCC bond angles were also calculated to visualize the geometric relaxation of the singlet intermediates after the vertical ISC event (see Figure 5). As expected, cyclization toward cyclopropanone is found to have only a small barrier. The

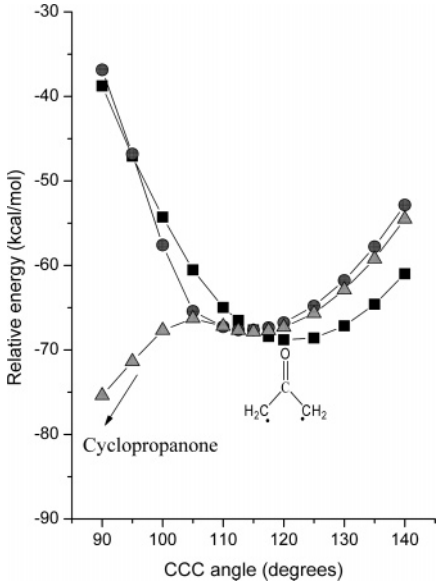

Figure 5. Potential energy curves around the crossing seam for oxyallyl as relevant for O-attack on the central carbon atom. Squares: energies of triplet **Int1a** optimized at fixed C−C−C angles; circles: energies of singlet wave functions calculated on the optimized triplet geometries (i.e. vertical transition from triplet to singlet surface); triangles: energies of singlet **Int11** optimized at fixed C−C−C angles, showing a negligible barrier to cyclization.

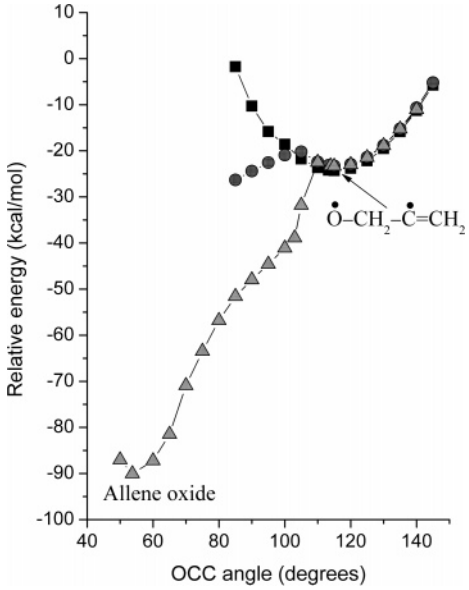

Figure 6. Potential energy curves around the crossing seam for oxyallene as relevant for the case of O-attack on a terminal carbon atom. Squares: energies of triplet **Int2a** optimized at fixed C−C−O angles; circles: energies of singlet wave functions calculated on the optimized triplet geometries (i.e. vertical transition from triplet to singlet surface); triangles: energies of singlet **Int13** optimized at fixed C−C−O angles, showing a negligible barrier to cyclization.

relative importance of surface crossing versus reactions on the triplet surface depends on the temperature, with the latter more favorable at higher temperatures, and the former predominant at low to moderate temperatures. For example, at 300 K rate for decomposition of **Int1a** is estimated to $\sim 2 \times 10^9$ s^{-1}, much slower than the rate of ISC (estimated at ca. 10^{11} s^{-1}), while decomposition at the average energy at 2000 K (rate $\approx 8 \times 10^{11}$ s^{-1}) is much faster than ISC. Accurate dynamic calculations are certainly required in order to quantify these two competing reaction steps, but these are outside the scope of the present work.

The subsequent reactions of the singlet intermediates thus formed are shown in Figure 3. Singlet oxyallyl **Int11** will undergo ring-closure to singlet cyclopropanone, **Int12**, with an energy of −99.9 kcal/mol relative to the initial reactants (see Figure 3). This step goes through **TS31** and faces a smaller barrier of 0.4 kcal/mol obtained at the CASSCF level,[51] and that the reaction is even barrierless when dynamic electron correlation was taken into account using the CASPT2 method.[51] Hence, the **Int11** → **Int12** step has a very small to nonexistent barrier, and in any case will be very rapid given the chemical activation of **Int11** arising after the ISC process. **Int11** could also undergo ring-closure leading to singlet allene oxide, **Int13**. However, this pathway goes via a tighter **TS32** with a higher barrier of ∼7 kcal/mol and so cannot compete with the **Int11** → **TS31** → **Int12** route.

Under high-pressure conditions, singlet cyclopropanone **Int12** can be thermally stabilized; it was observed in a matrix study.[9] At low pressures, **Int12** will either decompose to yield CO + C_2H_4 via **TS33** or isomerize to methylketene **Int15** via **TS34** or to 2-propanal **Int16** via **TS35**. The barrier heights for these three pathways are 36.4, 53.4, and 63.5 kcal/mol, respectively. As, moreover, **TS33** is looser than the other two, this results in predominance for the **Int12** → **TS33** → CO + C_2H_4 channel, in good agreement with the experimental observations.[7−12] Note that because both **TS31** and **TS33** lie far below the initial reactants and only slightly above the initial singlet intermediate **Int11**, the chemically activated **Int11** will isomerize in less than a picosecond to **Int12** which in turn will decompose equally promptly to end products (or be collisionally stabilized at very high pressures), such that in any case the probability of occurrence of a reverse ISC of singlet **Int11** back to triplet **Int1a** will be strongly reduced.

We also carried out an analogous CASPT2//CASSCF study of the crossing seam around the equilibrium structure of triplet biradical adduct oxyallene **Int2a** (see Figure 6), where the C−C−O bond angle was found to be the most significant difference between the singlet and triplet surfaces. The vertical energy gap between triplet and singlet surfaces, calculated from the energies of triplet biradical •O−CH_2−•C═CH_2 geometries (**Int2a**) optimized for fixed CCO bond angles versus the energies of singlet wave functions on these same geometries, is only a few kcal/mol for bond angles above 100°. The proximity of singlet and triplet PES enhances the probability of an ISC event allowing the formation of singlet intermediates. Energies of reoptimized singlet •O−CH_2−•C═CH_2 intermediates (**Int13**) as a function of the CCO bond angle (see Figure 6) show a negligible barrier to cyclization yielding allene oxide. Note that the lifetime of triplet oxyallene is so short, i.e., ∼10 ps at 300 K and quickly reducing to ∼1 ps at 1000 K, that an ISC process is likely to occur only at low to moderate temperatures (<1000 K). As a result, decompositions of **Int2a** with spin-conservation are expected to be the principal pathways at combustion temperatures. Singlet allene oxide formed from the fast cyclization reaction after ISC can either be stabilized under high-pressure conditions—as observed in the mentioned matrix study[9]—or isomerized on the singlet surface at lower pressures. **Int13** can undergo ring-opening to **Int11**, followed by rapid rearrangement to **Int12** and subsequent decomposition to products CO + C_2H_4. The **Int13** → **TS32** → **Int11** pathway faces a barrier of 30.3 kcal/mol, i.e., only half the 59.6 kcal/mol barrier to **Int13** → **TS37** → **Int16**. As a result, the first pathway, yielding CO + C_2H_4, is dominant under all relevant temperatures.

TABLE 2: Calculated Product Distribution at $P = 1$ Atm as a Function of Temperature for the $O(^3P) + CH_2{=}C{=}CH_2$ Reaction Occurring on the Triplet Surface after O-Addition on the Central Carbon[a]

	temperature (K)						
products	300	500	650	800	1000	1500	2000
$^3[OC_3H_4]$[b]	26.4	8.5	3.5	1.4	0.5	0.1	0.0
$O + C_3H_4$	0.0	0.0	0.0	0.0	0.0	0.0	0.0
$^3CH_2 + H_2CCO$	71.6	87.1	90.6	91.5	91.4	89.9	88.5
$^\bullet CH_3 + HC^\bullet CO$	0.6	1.8	2.6	3.1	3.4	3.5	3.4
$^\bullet OH + H_2C^\bullet CCH$	1.4	2.6	3.3	4.0	4.7	6.5	8.1

[a] See Figure 1. [b] Sum of yields of collisionally stabilized triplet OC_3H_4 species.

TABLE 3: Calculated Product Distribution at $P = 1$ Atm as a Function of Temperature for the $O(^3P) + CH_2{=}C{=}CH_2$ Reaction Occurring on the Triplet Surface after O-Addition on a Terminal Carbon[a]

	temperature (K)						
products	300	500	650	800	1000	1500	2000
$^3[OC_3H_4]$[b]	14.5	4.1	1.6	0.7	0.2	0.0	0.0
$O + C_3H_4$	0.0	0.1	0.2	0.4	0.6	1.4	2.0
$CH_2{=}C^\bullet CHO + {}^\bullet H$	40.1	49.9	56.8	62.5	68.1	77.7	82.2
$^3CH_2 + H_2CCO$	37.8	36.9	31.8	26.7	21.3	11.8	7.4
$CH_2{=}CH^\bullet CO + {}^\bullet H$	4.5	5.1	5.4	5.6	5.7	5.7	5.5
$HC^\bullet O + {}^\bullet C_2H_3$	1.1	1.3	1.4	1.5	1.6	1.7	1.8
$CO + {}^3C_2H_4$	0.4	0.4	0.4	0.4	0.4	0.3	0.2
$^\bullet CH_3 + HC^\bullet CO$	0.3	0.7	0.9	0.8	0.7	0.4	0.2
$^\bullet OH + H_2C^\bullet CCH$	0.5	0.7	0.8	0.8	0.8	0.6	0.4
$CO + {}^3CH_3CH$	0.8	0.8	0.7	0.6	0.5	0.4	0.3

[a] See Figure 2. [b] Sum of yields of collisionally stabilized triplet OC_3H_4 species.

In summary, crossing seams were located for intermediates formed in both the central and terminal O-additions to allene; the intersystem crossings from triplet to the lowest-lying singlet surface can lead to vibrationally hot cyclopropanone and allene oxide intermediates. The contribution of these ISC processes is sensitive to the reaction temperature and is predicted to be important mostly at low temperatures. The hot singlet intermediates will decompose entirely into $CO + C_2H_4$ under low-pressure conditions but become thermally stabilized at high pressures. The predicted products singlet cyclopropanone, allene oxide, CO, and C_2H_4, were all observed experimentally.[9,10]

III.2. Quantification of the Product Distribution. The overall product distribution of the title reaction can be obtained from the weighted summation of the product distributions for the different, site-specific entrance channels. These channel-specific product distributions as well as the contributions of the different O-addition and H-abstraction channels to the overall rate coefficient are functions of temperature (see e.g. Figure 4). In the following section, we will discuss product distributions predicted for the different entrance channels as proceeding on an adiabatic triplet surface. Note that the entire triplet PES is included in all the master equation analyses, i.e., both regions shown in Figures 1 and 2 are included in the kinetic reaction scheme at all times.

O-Atom Attack on the Central Carbon. Various product branching ratios computed at $P = 1$ atm as a function of temperature are tabulated in Table 2. As can be seen, triplet methylene plus ketene are the major products with very high yields, ca. 90% at $T \geq 500$ K. All other products show minor yields. These results are a direct consequence of the low-lying **Int1a** → **TS4** → $^3CH_2 + H_2CCO$ channel, with **TS4** a loose transition structure. At low temperatures, the yield of stabilized triplet oxyallyl becomes important, ca. 26% at 300 K. In contrast, its yield is negligible at higher temperatures. We performed some sample calculations at higher pressures to locate the onset of the falloff region for a "combustion" temperature, $T = 1500$ K, but found only a small fraction of stabilization for triplet oxyallyl (<8%) even at $P = 100$ atm. This result was expected as the lifetime of triplet oxyallyl is estimated to be so short (~5 ps at $T = 1500$ K) and given that it requires many collisions to bring a vibrationally hot triplet oxyallyl below the lowest-lying decomposition transition structure. Thermally stabilized triplet oxyallyl is predicted to then undergo an ISC step, followed by ring-closure to lead to singlet cyclopropanone.

O-Atom Attack on a Terminal Carbon. Various product distributions obtained at $P = 1$ atm as a function of temperature are presented in Table 3. The products $CH_2{=}C^\bullet{-}CHO + H^\bullet$ and $^3CH_2 + H_2CCO$ clearly dominate. While the former products arise from O-addition on a terminal carbon (see Figure 2), the latter result from O-attack on the central carbon (see Figure 1). At $T = 300$ K, the yields of these two products are almost equivalent. The yield of products $CH_2{=}C^\bullet{-}CHO + H^\bullet$ sharply rises with increasing temperatures, from 40% at 300 K up to 82% at 2000 K, whereas the yield of products $^3CH_2 + H_2CCO$ drops sharply with increasing temperatures, from 38% at 300 K down to 7% at 2000 K.

At 1 atm and at room temperature, a 15% yield is calculated for stabilized triplet oxyallyl, which after ISC and ring-closure gives rise to singlet cyclopropanone. However, this yield becomes very minor (≤ 3%) at high temperatures ($T \geq 1500$ K) even at $P = 100$ atm. Note that the yield of $CH_2{=}CH{-}^\bullet CO + H^\bullet$ is minor, ca. 5%, and almost temperature-independent, indicating that the experimentally observed $^\bullet C_3H_3O$ species[10] corresponds to the more abundant $CH_2{=}C^\bullet{-}CHO$ isomer formed by O-addition on the central carbon.

As already mentioned, singlet cyclopropanone and/or singlet allene oxide formed from ISC processes should almost entirely decompose to yield $CO + C_2H_4$, except at very high pressures. Other products from the singlet PES are predicted to be all very minor, with yields less than 5%. Note that $CO + C_2H_4$ can be formed from both addition sites at low temperatures. At higher temperatures $CO + C_2H_4$ will only be formed from triplet oxyallyl following O-attack on the central carbon. Considering that the fraction of O-addition on the central carbon has a negative temperature-dependence (see Figure 4), the yield of $CO + C_2H_4$ is predicted to be considerably reduced when temperature increases substantially.

A quantitative prediction of the overall product branching ratios spanning all potential energy surfaces is at this time difficult due to the need for accurate dynamic calculation on the rate of the ISC process. For these systems such calculations are extremely demanding and beyond our current computational resources. An alternative approach used successfully in earlier work,[4,5] where the ratio of ISC crossing versus on-surface unimolecular reactions is calibrated against experimental measurements, is not possible here due to the current lack of sufficiently complete experimental product distribution data.

III.3. Overall Thermal Rate Coefficient. The overall temperature-dependent rate coefficient $k(T)_{overall}$ for the $O(^3P) + CH_2{=}C{=}CH_2$ reaction can be computed according to the following expression

$$k(T)_{overall} = k(T)^{TST}_{O-add-cen} + k(T)^{TST}_{O-add-ter} + k(T)^{TST}_{H-abs} \quad (12)$$

where $k(T)^{TST}$ is the rate coefficient derived from multistate transition state theory

$$k(T)^{\mathrm{TST}}_{\mathrm{O-add-en}} = \frac{k_b T}{h} \times \frac{(1-\gamma_{\mathrm{TS1a}}) \times Q^{\ddagger}_{\mathrm{TS1a}} \times \exp(-E_{\mathrm{TS1a}}/RT) + (1-\gamma_{\mathrm{TS1b}}) \times Q^{\ddagger}_{\mathrm{TS1b}} \times \exp(-E_{\mathrm{TS1b}}/RT)}{Q_{\mathrm{O}} Q_{\mathrm{C_3H_4}}}$$

$$k(T)^{\mathrm{TST}}_{\mathrm{O-add-ter}} = \frac{k_b T}{h} \times \frac{(1-\gamma_{\mathrm{TS2a}}) \times Q^{\ddagger}_{\mathrm{TS2a}} \times \exp(-E_{\mathrm{TS2a}}/RT) + (1-\gamma_{\mathrm{TS2b}}) \times Q^{\ddagger}_{\mathrm{TS2b}} \times \exp(-E_{\mathrm{TS2b}}/RT)}{Q_{\mathrm{O}} Q_{\mathrm{C_3H_4}}}$$

and

$$k(T)^{\mathrm{TST}}_{\mathrm{H-abs}} = \frac{k_b T}{h} \times \frac{\kappa_{\mathrm{TS3a}} \times Q^{\ddagger}_{\mathrm{TS3a}} \times \exp(-E_{\mathrm{TS3a}}/RT) + \kappa_{\mathrm{TS3b}} \times Q^{\ddagger}_{\mathrm{TS3b}} \times \exp(-E_{\mathrm{TS3b}}/RT)}{Q_{\mathrm{O}} Q_{\mathrm{C_3H_4}}}$$

where $Q(T)$ is a complete partition function, k_b is Boltzmann's constant, h is Planck's constant, R is the universal gas constant, E_{TS} is the internal energy of a transition structure relative to the initial reactants, κ is the one-dimensional tunneling correction computed by assuming an asymmetric Eckart potential,[48,49] and γ^{re} is the fraction of redissociation of the initial adducts back to the initial reactants, function of temperature and pressure (see Tables 2 and 3). At low temperatures, redissociation is negligible and the value of γ^{re} is close to 0. Above 1000 K, redissociation becomes non-negligible, but its contribution is the result of a complicated competition among the redissociation reactions, further isomerization, and IC/ISC processes (IC for **Int1b** and **Int2b)**. Accurate quantification of γ^{re} therefore again requires dynamic calculations, which are beyond the scope of this paper. We therefore limited ourselves to the calculation of $k(T)_{overall}$ at $T \leq 1000$ K; for these lower temperatures experimental data are available for comparison. The rotational symmetries for allene and the transition states are 4 and 1, respectively, such that the reaction path degeneracy is 4 for each channel, as already discussed earlier. The electronic partition function of the O atom explicitly includes the three lowest-lying electronic states ($^3P_2$ with electronic degeneracy $g = 5$, $^3P_1$ with $g = 3$, and $^3P_0$ with $g = 1$), with relative energies of 0.0000, 0.4525, and 0.6490 kcal/mol, respectively.[52] Also, the electronic degeneracy of 3 for the transition structures, having a triplet electronic state, is duly taken into account.

The rate predictions are plotted in Figure 7 and can be well-reproduced by a modified Arrhenius equation $1.60 \times 10^{-17} \times T^{2.05} \times \exp(-90/T)$ cm^3 molecule^{-1} s^{-1}; the most recent experimental data are also shown for comparison. Our $k(T)$ results are in near-perfect agreement with the experimental values obtained by Cvetanovic and co-workers[6,14] over the entire range 300−600 K, while they are overestimations compared to measurements by Atkinson[13] and by Aleksandrov.[15] At room temperature, our predicted rate coefficient is 1.4×10^{-12} cm^3 molecule^{-1} s^{-1}, in excellent agreement with the recommended value of 1.3×10^{-12} cm^3 molecule^{-1} s^{-1} in the literature,[6] but is an overestimation by ca. 30% of the 1.0×10^{-12} cm^3 molecule^{-1} s^{-1} measurement by Atkinson.[13] Increasing relative energies for all O-addition and H-abstraction transition structures on the triplet surface by 0.1 kcal/mol will bring $k(T)$ values slightly down to between the experimental $k(T)$ data observed by Nip[14] and by Atkinson[13] (see Figure S15, Supporting Information). Theoretical $k(T)$ values are quite sensitive to the accuracy of barrier heights, especially at low temperatures: at room temperature a difference in barrier height by 0.5 kcal/mol alters the computed $k(T)$ values by a factor of 2.3. Further experimental studies are recommended for a more precise determination of the rate coefficient.

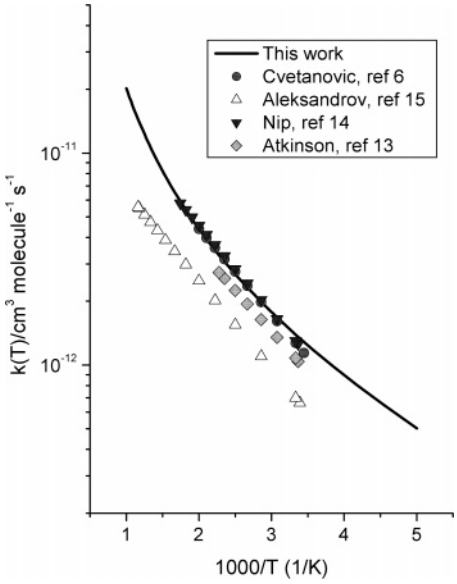

Figure 7. Overall thermal rate coefficients for the O(^{3}P) + allene reaction: comparison between experimental data and the current theoretical predictions.

IV. Concluding Remarks

In the present theoretical study, the lowest-lying triplet and singlet potential energy surfaces for the O(^{3}P) + CH_2=C=CH_2 reaction were characterized uniformly using the high level quantum chemical CBS-QB3 method. RRKM-master equation calculations, to evaluate primary product distribution for each of these surfaces and to qualitatively predict the overall major products, were carried out using the exact stochastic simulation method. In addition, overall thermal rate coefficients were determined in the 200−1000 K range using multistate transition state theory. A number of important results emerge from this study and can be summarized as follows:

(i) The O(^{3}P) + CH_2=C=CH_2 reaction is confirmed to occur dominantly but not exclusively via an electrophilic addition mechanism as the first reaction step. The predicted major products from these addition reactions are CO + C_2H_4, $^3CH_2$ + H_2CCO, and CH_2=C$^{\bullet}$−CHO + H$^{\bullet}$. CO + C_2H_4 are mainly produced from the lowest-lying singlet surface following an ISC process and can be formed from both addition channels; these results confirm earlier experimental observations. $^3CH_2$ + H_2CCO can likewise be formed from O-attack on the central and terminal carbons, whereas CH_2=C$^{\bullet}$−CHO + H$^{\bullet}$ are nearly exclusively products of O-addition on a terminal carbon.

(ii) The H-abstraction reaction proceeds on two electronic surfaces, $^3A''$ and $^3A'$, and results in OH($X^2\Pi$) + $H_2C^{\bullet}$−C≡CH products, predicted to be important at high temperatures. The contributions of H-abstraction to the overall product formation are estimated to be ca. 35% at 2000 K.

(iii) The entrance barrier heights and reaction enthalpies computed at the CBS-QB3 level of theory are in better agreement with available experimental data compared to previous theoretical results.

(iv) The lack of accurate dynamic calculations for ISC rates and/or of available experimental product branching ratios prohibits us from quantitatively predicting the overall primary product distribution for the title reaction. However, the present

study elucidates the reaction mechanism and qualitatively predicts the major products.

(v) The computed overall TST rate coefficient for the range 200−1000 K: $k(T) = 1.60 \times 10^{-17} \times T^{2.045} \times \exp(-90.5\ \mathrm{K}/T)$ cm^3 $\mathrm{molecule}^{-1}$ s^{-1}, is in excellent agreement with the experimental data in the literature.

Acknowledgment. The authors are indebted to the FWO-Vlaanderen and the KULeuven Research Council (BOF fund) for continuing financial support. T.L.N. and L.V. thank the KULeuven Research Council for a Ph.D. scholarship and a postdoctoral mandate, respectively.

Supporting Information Available: Optimized geometries, zero-point energies, rotational constants, harmonic vibration frequencies, various graphs of IRC calculations, and orbitals of key intermediates . This material is available free of charge via the Internet at http://pubs.acs.org.

References and Notes

(1) Glassman, I. *Combustion*, 2nd ed.; Academic Press: Florida, 1987.
(2) Gardiner, W. C., Jr. *Combustion Chemistry*; Springer-Verlag: New York, 1984.
(3) Nguyen, T. L.; Vereecken, L.; Peeters, J. *J. Phys. Chem. A* **2006**, in press.
(4) Nguyen, T. L.; Vereecken, L.; Hou, X. J.; Nguyen, M. T.; Peeters, J. *J. Phys. Chem. A* **2005**, *109*, 7489.
(5) Nguyen, T. L.; Dils, B.; Carl, S. A.; Vereecken, L.; Peeters, J. *J. Phys. Chem. A* **2005**, *109*, 9786.
(6) Cvetanovic, R. J. *J. Phys. Ref. Data* **1987**, *16*, 261.
(7) Havel, J. J. *J. Am. Chem. Soc.* **1974**, *96*, 530.
(8) Lin, M. C.; Shortridge, R. G.; Umstead, M. E. *Chem. Phys. Lett.* **1976**, *37*, 279.
(9) Singmaster, K. A.; Pimentel, G. C. *J. Mol. Struct.* **1989**, *194*, 215.
(10) Schmoltner, A. M.; Huang, S. Y.; Brudzynski, R. J.; Chu, P. M.; Lee, Y. T. *J. Chem. Phys.* **1993**, *99*, 1644.
(11) Xing, G.; Huang, X.; Wang, X.; Bersohn, R. *J. Chem. Phys.* **1996**, *105*, 488.
(12) Herbrechtsmeier, V. P.; Wagner, H. G. *Ber. Bunsen-Ges. Phys. Chem.* **1972**, *76*, 517.
(13) Atkinson, R.; Pitts, J. N., Jr. *J. Chem. Phys.* **1977**, *67*, 2492.
(14) Nip, W. S.; Singleton, D. L.; Cvetanovic, R. J. *Can. J. Chem.* **1979**, *57*, 949.
(15) Aleksandrov, E. N.; Arutyunov, V. S.; Kozlov, S. N. *Kinet. Catal.* **1980**, *21*, 1327.
(16) From NIST Web page: http://srdata.nist.gov/cccbdb/.
(17) Chiu, Y. N.; Abidi, M. S. F. A. *J. Phys. Chem.* **1982**, *86*, 3288.
(18) Hammond, B. L.; Huang, S. Y.; Lester, W. A., Jr.; Dupuis, M. *J. Phys. Chem.* **1990**, *94*, 7969.
(19) Becke, A. D. *J. Chem. Phys.* **1993**, *98*, 5648.
(20) Stevens, P. J.; Devlin, F. J.; Chablowski, C. F.; Frisch, M. J. *J. Phys. Chem.* **1994**, *98*, 11623.
(21) Gonzalez, C.; Schlegel, H. B. *J. Chem. Phys.* **1989**, *90*, 2154.
(22) Gonzalez, C.; Schlegel, H. B. *J. Phys. Chem.* **1990**, *94*, 5523.
(23) Montgomery, J. A., Jr.; Frisch, M. J.; Ochterski, J. W.; Petersson, G. A. *J. Chem. Phys.* **1999**, *110*, 2822.
(24) Werner, H. J.; Knowles, P. J. *J. Chem. Phys.* **1985**, *82*, 5053.
(25) Knowles, P. J.; Werner, H. J. *Chem. Phys. Lett.* **1985**, *115*, 259.
(26) Celani, P.; Werner, H. J. *J. Chem. Phys.* **2000**, *112*, 5546.
(27) Frisch, M. J.; Trucks, G. W.; Schlegel, H. B. et al. *Gaussian 03*; Gaussian, Inc.: Pittsburgh, PA, 2004.
(28) DALTON, a molecular electronic structure program, written by Helgaker T.; Jensen, H. J. Aa.; Joergensen, P.; Olsen, J.; Ruud, K.; Aagren, H.; Auer, A. A. et al., Release 1.2, 2001.
(29) MOLPRO is a package of ab initio programs written by Werner, H.-J.; Knowles, P. J.; Schütz, M.; Lindh, R.; Celani, P.; Korona, T.; Rauhut, G.; Manby, F. R.; Amos, R. D.; Bernhardsson, A.; Berning, A.; Cooper, D. L.; Deegan, M. J. O.; Dobbyn, A. J.; Eckert, F.; et al. 2002.
(30) Gillespie, D. T. *J. Comput. Phys.* **1976**, *22*, 403.
(31) Gillespie, D. T. *J. Phys. Chem.* **1977**, *81*, 2340.
(32) Gillespie, D. T. *J. Comput. Phys.* **1978**, *28*, 395.
(33) Vereecken, L.; Huyberechts, G.; Peeters, J. *J. Chem. Phys.* **1997**, *106*, 6564.
(34) Matsumoto, M.; Nishimura, T. *ACM Trans. Model. Comput. Simul.* **1998**, *8*, 3.
(35) Hippler, H.; Troe, J.; Wendelken, H. J. *J. Chem. Phys.* **1983**, *78*, 6709.
(36) Troe, J. *J. Chem. Phys.* **1977**, *66*, 4745.
(37) Forst, W. *Theory of Unimolecular Reactions*; Academic Press: New York, 1973.
(38) Robinson, P.; Holbrook, K. *Unimolecular Reactions*; Wiley-Interscience: London, 1972.
(39) Gilbert, R. G.; Smith, C. S. *Theory of Unimolecular and Recombination Reactions*; Blackwell Scientific: Oxford, 1990.
(40) Holbrook, K.; Pilling, M.; Robertson, S. *Unimolecular Reactions*, 2nd ed.; Wiley: New York, 1996.
(41) Steinfeld, J. I.; Francisco, J. S.; Hase, W. L. *Chemical Kinetics and Dynamics*; Prentice Hall: Englewood Cliffs, NJ, 1999.
(42) Baer, T.; Hase, W. L. *Unimolecular Reaction Dynamics: Theory and Experiment*; Oxford University Press: Oxford, 1996.
(43) Beyer, T.; Swinehart, D. F. *Comm. Assoc. Comput. Machines* **1973**, *16*, 379.
(44) Stein, S. E.; Rabinovitch, B. S. *J. Chem. Phys.* **1973**, *58*, 2438.
(45) Klessinger, M.; Michl, J. *Excited States and Photochemistry of Organic Molecules*; VCH: New York, 1995.
(46) Haas, Y.; Klessinger, M.; Zilberg, S. *Chem. Phys.* **2000**, *259*, 121 and references therein.
(47) Roth, W. R.; Hoff, H.; Horn, C. *Chem. Ber.* **1994**, *127*, 1781.
(48) Eckart, C. *Phys. Rev.* **1930**, *35*, 1303.
(49) Johnston, H. S.; Heicklen, J. *J. Phys. Chem.* **1966**, *66*, 532.
(50) Coolidge, M. B.; Yamashita, K.; Morokuma, K.; Borden, W. T. *J. Am. Chem. Soc.* **1990**, *112*, 1751.
(51) Hess, B. A., Jr.; Eckart, U.; Fabian, J. *J. Am. Chem. Soc.* **1998**, *120*, 12310.
(52) NIST Web page: http://physics.nist.gov/PhysRefData/Handbook/periodictable.htm.